NACA

RESEARCH MEMORANDUM

EFFECT OF JET-NOZZLE-EXPANSION RATIO ON DRAG OF PARABOLIC AFTERBODIES

By Gerald W. Englert, Donald J. Vargo, and Robert W. Cubbison

Lewis Flight Propulsion Laboratory
Cleveland, Ohio

NATIONAL ADVISORY COMMITTEE
FOR AERONAUTICS

WASHINGTON
April 19, 1954

NATIONAL ADVISORY COMMITTEE FOR AERONAUTICS

RESEARCH MEMORANDUM

EFFECT OF JET-NOZZLE-EXPANSION RATIO ON DRAG OF PARABOLIC AFTERBODIES

By Gerald W. Englert, Donald J. Vargo, and Robert W. Cubbison

SUMMARY

Three exit-nozzle-afterbody configurations were investigated in the Lewis 8- by 6-foot supersonic wind tunnel at Mach numbers of 2.0, 1.6, and 0.6 and over a range of pressure ratio. The three nozzles used included one convergent and two convergent-divergent types, the latter having expansion ratios of 1.44 and 1.83, respectively. All boattails were of a parabolic contour, and base regions were kept small.

Study of the total afterbody-drag values at supersonic speeds indicated that over most of the high-pressure-ratio range increasing the nozzle design expansion ratio increases the drag even though the boattail area is reduced.

The influence of the jet on boattail drag was very pronounced; for instance, at a free-stream Mach number of 1.6, changes in boattail pressures were experienced as far forward as 1 jet diameter. At a free-stream Mach number of 0.6, the jet effect was propagated over all the boattail surface.

Base pressure was strongly affected by the interaction of the external flow and the internal jet stream. For all three configurations, increasing the pressure ratio from a jet-off condition first caused the base drag to increase and then to decrease, finally producing a negative drag. In general, base pressure was decreased with increase of angle of attack.

Increasing the pressure ratio tended to increase slightly the total-drag increment caused by angle-of-attack operation.

INTRODUCTION

Considerable work has been done on the afterbody drag of various axially symmetric configurations with and without blunt bases (refs. 1 to 6). Later investigations (refs. 7 to 10), in which all or part of the blunt base has been replaced by an exhaust nozzle or bleed holes, have shown that considerable reduction in afterbody drag can be obtained because of the presence of flow in the base region.

Greater knowledge of the magnitude of the effects of internal flow upon afterbody drag is becoming mandatory with the increasing demands imposed upon the performance of supersonic airplanes and missiles. The flight speeds associated with these vehicles are usually coincident with a wide pressure-ratio range across the nozzle of the propulsion equipment. The nozzle and afterbody configuration must be one which combines these components into a configuration with optimum thrust-minus-drag characteristics. For a given throat area, changes in nozzle-expansion ratio often require geometrical changes in boattail geometry. Since the afterbody drag can be a large percentage of the total drag of airplanes and missiles, these boattail changes must be carefully evaluated.

This report presents the results of an investigation undertaken in the Lewis 8- by 6-foot supersonic wind tunnel to study the effects of nozzle-expansion ratios on afterbody drag. One convergent and two convergent-divergent nozzles were used in conjunction with parabolic external boattail fairings. The nozzle-expansion ratios were 1.00, 1.44, and 1.83 and correspond to design pressure ratios (inlet total pressure divided by average exit static pressure) of $\leq$1.89, 5.75, and 9.10, and average exit Mach numbers of $\leq$1.00, 1.80, and 2.10, respectively, for a ratio of specific heats of 1.4 and isentropic flow.

These exit configurations were studied over a range of nozzle pressure ratio from jet off to values in excess of 12 at free-stream Mach numbers of 2.0, 1.6, and 0.6. Some data at angles of attack of 4° and 8° were also obtained. The Reynolds number based on model length and free-stream flow varied from 2.14×10^7 to 3.24×10^7.

SYMBOLS

The following symbols are used in this report:

A	area, sq ft
C_D	drag coefficient based on maximum body area

C_p	pressure coefficient, $\frac{p - p_0}{q_0}$
D	diameter, in.
L	nozzle length, in.
M	Mach number
P	total pressure, lb/sq ft
p	static pressure, lb/sq ft
P_1/p_0	nozzle pressure ratio
q	dynamic pressure, $\gamma pM^2/2$, lb/sq ft
R	radius, in.
x	distance, in.
α	angle of attack, deg
γ	ratio of specific heats

Subscripts:

a	boattail
b	base
e	nozzle exit
f	friction
m	maximum
N	nozzle
n	nose
p	pressure
t	total

0 free stream

1 nozzle entrance

APPARATUS AND PROCEDURE

The basic apparatus employed was a body of revolution supported in the wind-tunnel test section by two hollow struts (fig. 1(a)). The body consisted of a parabolic nose, a cylindrical centerbody, and the afterbody and exit-nozzle configuration being evaluated. The hollow support struts served the additional purpose of ducting high-pressure air into the model. After entering the model this air was turned 90°, passed through a honeycomb flow straightener, and then discharged through the test nozzle. To avoid the possible formation of condensation shocks in the nozzle, the air was preheated to 400° F.

The basic body had a maximum diameter of 8.25 inches and was kept at a length of 83.75 inches including the afterbodies. It was so mounted that the rear portion of the afterbody and part of the jet could be viewed from schlieren windows mounted in the tunnel walls.

A strain-gage-type balance was located within the forebody of the model. With one side of the balance fixed or grounded to the support struts, the entire outer fairing of the basic body was attached to the free or measuring side of the balance (see fig. 1(b)). Balance-derived drag forces were compared with forces obtained by an integration of static pressures measured on various sections of the model. A more detailed analysis of the data-reduction techniques employed is presented in reference 11.

A basic convergent section served as one of the nozzles as well as the subsonic, or convergent, section of the two convergent-divergent nozzles. The contour of this section was such that the acceleration of the air versus the axial distance x from the nozzle entrance to throat followed the trignometric function $\alpha = \frac{k}{L}\left(1 - \cos\frac{2\pi n}{L}\right)$ (based on a one-dimensional flow analysis). In this equation L equals the length of the convergent section and k equals the velocity at the throat squared minus the velocity at the nozzle entrance squared. This procedure yields a smooth bellmouth type of nozzle. The remaining two nozzles consisted of this basic converging section to which was added two different diverging sections, having area expansion ratios of 1.44 and 1.83, respectively. Based on one-dimensional flow analysis, the diverging sections were arbitrarily contoured such that the air accelerated at a

constant rate of change of Mach number per inch of axial distance, $dM/dx = 0.4$. As is illustrated in figure 1(c), these nozzles with expansion ratios of 1.00, 1.44, and 1.83 will hereinafter be referred to as nozzles A, B, and C, respectively.

The boattail surrounding each nozzle had the profile of a parabola of revolution cut off normal to the axis of symmetry at three different locations to fit the nozzle-exit diameters. By varying the length of the upstream cylindrical section, the trailing edges of each nozzle and its corresponding boattail were located in the same plane for all three configurations. A clearance of 0.1 inch between the boattail inner surface and nozzle outer surface was maintained.

The pressure ratio across the nozzle P_1/p_0 was varied from the maximum available to a jet-off condition.

Data were obtained at free-stream Mach numbers of 2.0, 1.6, and 0.6 at an angle of attack of zero. Some data were also obtained at angles of attack of 4° and 8° at free-stream Mach numbers of 1.6 and 2.0.

Numerous static-pressure orifices were located along the top, bottom, and side boattail surfaces and in the throat and diverging sections of the nozzle, as is illustrated in figure 1(d). Base pressure was measured by means of three static-pressure taps located in the annulus between the boattail and nozzle walls.

As part of this study, a run was also made to survey the afterbody boundary layer in the region of the nozzle exit (fig. 1(e)). For this run only, five radial boundary-layer rakes of five total-head tubes each were mounted at the 90° (top), 135°, 180°, 225°, and 270° circumferential locations.

RESULTS AND DISCUSSION

Initially, the afterbody drag components (pressure drag of the boattail, base drag, and friction drag of the boattail) are discussed. A summation of these components is then made and compared with an independently determined total drag calculated from the strain-gage balance measurements.

Boattail Pressure Drag

The experimental boattail-pressure-drag coefficients $C_{D_{a,p}}$ of the three nozzles are presented in figure 2 as a function of the pressure

ratio P_1/p_0. These data are for zero angle of attack at free-stream Mach numbers of 0.6, 1.6, and 2.0 and were obtained from the area averages of the local pressure coefficients

$$C_{D_{a,p}} = \frac{2}{R_{a,m}^2} \int_{R_{b,m}}^{R_{a,m}} C_p R \, dR$$

which were calculated from boattail pressure surveys similar to that presented in figure 3. The curves were faired to zero pressure coefficient for the supersonic-flow cases at the point where the boattailing starts. The pressure tap upstream of this point was at free-stream pressure indicating that the disturbance of the forebody had dissipated.

Since the throat areas of all three nozzles were the same, the boattail area projected in an axial direction decreased with an increase in the nozzle expansion ratio. Of the three nozzles investigated, the supersonic pressure drag in the jet-off condition was therefore highest for nozzle A and least for nozzle C. In general, as the nozzle pressure ratio was increased, the jet influence on external flow caused the static pressures on the boattail to rise, lowering the boattail drag considerably. The jet effect was, in fact, so pronounced that negative drag was obtained for the convergent nozzle configuration (nozzle A) at free-stream Mach numbers of 1.6 and 0.6 at pressure ratios above 10.0 and 4.3, respectively. Because of this interaction, increasing the design expansion ratio at high pressure ratio increased the boattail pressure drag even though the boattail area was decreased.

The external air flowing in a converging direction along the afterbody must make an abrupt change in direction when it encounters the nozzle jet stream. An oblique shock wave forms in the stream flow (fig. 4), and because of the presence of boundary layer on the boattail surface, the pressure rise across the shock is transmitted upstream of the point of intersection of the shock wave and afterbody (ref. 10). Because of the adverse pressure gradient, the boundary layer is thickened and the shock pattern fans out into multiple shocks along the boattail surface. The regions of rapidly increasing pressure coefficient along the rear of the boattail (fig. 3 for example) confirm this analysis. When the pressure ratio across a given nozzle is considerably greater than the design pressure ratio, the average internal static pressure at the nozzle exit is greater than free stream, and the nozzle is said to be underexpanded. In this case, the flow continues to expand as it flows beyond the nozzle exit which causes an increase of strength of the previously mentioned shock wave and forces it further forward on the boattail surface. This in turn results in a greater reduction in boattail drag.

At a free-stream Mach number of 1.6, this jet effect propagated approximately 1 diameter upstream of the nozzle exit at a pressure ratio of 9 for nozzle B, which had a design pressure ratio of 5.75.

For the case where the stream is subsonic, the flow over the external boattail diffuses as it approaches the nozzle-exit station. As the nozzle pressure ratio is increased, the pressure rise in the flow about the boattail resembles that of the flow ahead of a body with increasing bluntness because of the increased spreading of the jet boundary. By referring again to figure 3, it can be seen that at a free-stream Mach number of 0.6 the jet influenced the pressure over the entire boattail of nozzle configuration B. Similar results were observed with the other nozzle configurations.

Some increase in drag with increase of nozzle pressure ratio at values of the jet pressure ratio considerably below design was indicated for nozzle C at both Mach numbers 2.0 and 1.6 (fig. 2). This increase may be due to entrainment effect. The entrainment of base air by the jet would increase the local velocity over the boattail surfaces and thus lower the local static pressure. A similar phenomenon may be encountered if, as a result of high boattail angle, the external flow is separated under jet-off condition and with jet on becomes reattached because of entrainment. The latter appears to be the case for nozzle B (fig. 3) at free-stream Mach numbers of 1.6 and 2.0. As the pressure ratio is further increased, the aspiration effect becomes small compared with the previously discussed large effect of the resulting shock pattern on the drag.

A comparison of the pressure distribution over the boattail of nozzle B with the results calculated by means of the potential-flow theory of references 12 and 13 is also shown in figure 3. Generally, good agreement was noted over most of the boattail. Since the theory was applied over the geometrical boundary of the boattail, with an assumption of no separation, disagreement results between theory and experiment over the rear portion of the boattail. Aside from flow separation, pressure feedback also occurs, resulting in a thickened boundary layer and a distortion of the originally assumed potential flow.

Base Drag

The effect of the jet flow upon the base pressures of the three configurations was quite similar to the jet-flow effect upon the rearmost boattail pressures. The pronounced aspiration effect of the jet at low pressure ratios is demonstrated in figure 5. Then, as the jet

[redacted]

pressure ratio is raised, the trend reverses and increasing base pressures are experienced, finally producing a negative drag.

The incremental change of base pressure coefficient due to angle-of-attack operation is presented as a function of nozzle pressure ratio in figure 6 at free-stream Mach numbers of 1.6 and 2.0. In general, increasing the angle of attack decreased the base pressure.

Friction Drag Coefficient

Because boundary-layer rakes were installed at the rearmost boattail station only (see APPARATUS AND PROCEDURE), the friction drag determined applies to the entire external body of revolution, plus any interference of the support struts. The friction drag values are plotted as a function of nozzle pressure ratio in figure 7. A slight downward trend in friction drag with increase of pressure ratio can be detected; however, this variation is probably within the accuracy of the data, as only a small region of the total body surface is influenced by the jet (indicated in figs. 3 and 4). The complex flow pattern and the possible interaction of the survey rake on the boundary layer added to the uncertainty of the accuracy. No friction-drag data were computed at a free-stream Mach number of 0.6 because of difficulties in computing the extent of the separation regions.

The wake survey aided in gaining some qualitative insight into how the interference of the support strut influenced the local flow-field distributions in the vicinity of the afterbody and nozzle exit. Resulting distributions for zero angle of attack are presented in figure 8 at high and low nozzle pressure ratios for free-stream Mach numbers of 2.0, 1.6, and 0.6. As is illustrated by the lines of constant Mach number enclosing the large band near the 180° region of the plots, the relative position and influence of the strut wake is clearly outlined.

Total Drag

Total drag values of the model fuselage obtained from strain-gage-balance measurements are presented in figure 9. At low pressure ratios and at the supersonic speeds studied, the total drag increased with decreasing nozzle design expansion ratio; whereas at high pressure ratios, the drag decreased with decreasing design expansion ratio. Because the forebody pressure drag is constant and the body total friction drag remained essentially constant with nozzle pressure ratio, the total drag exhibits the same general characteristic as the summation of the boattail and base drag coefficients.

Figure 10 is an independent check between the force measurements giving total drag and the independently determined component drags. The comparison is made by subtracting the friction drag of figure 7, the base drag from figure 5, and the theoretical forebody pressure drag computed by the method of reference 14 from the total drag in order to obtain boattail drag. This latter result is compared with the boattail drags (fig. 2) computed from pressure integration. Generally, good agreement in trend is observed. However, the absolute force values determined by subtraction at a free-stream Mach number of 1.6 were somewhat higher than the results obtained from pressure integration. Better agreement was noted at a free-stream Mach number of 2.0.

3155

The increment of total drag coefficient (determined with the balance) is presented as a function of nozzle pressure ratio in figure 11 at angles of attack of 4° and 8°. All three nozzle configurations seemed to have about the same angle-of-attack characteristics, since the data appear to fall on a single line. Increasing the pressure ratio tended to increase slightly the total-drag increment caused by angle-of-attack operation.

CE-2

The effect of the jet on forces normal to the model axis during angle-of-attack operation was also investigated. Within the range and accuracy of the data there appeared to be no effect for angles of attack up to 8°, the maximum investigated.

SUMMARY OF RESULTS

The drag of parabolic afterbodies surrounding one convergent and two convergent-divergent nozzles was investigated over a range of nozzle pressure ratio from a jet-off condition to a pressure ratio of 12 for free-stream Mach numbers of 1.6 and 2.0 and to a pressure ratio of 5 for a stream Mach number of 0.6. For these ranges of variables the following conclusions were reached:

1. The interaction of the jet on the boattail caused the boattail pressure drag to decrease markedly at high pressure ratios. Because of this interaction, increasing the design expansion ratio at high pressure ratio increased the boattail pressure drag even though the boattail area decreased because the nozzle throat area was fixed.

2. Base pressure was strongly affected by the internal air stream. In the low-pressure-ratio range, base pressure was decreased; but beyond a nozzle pressure ratio of 4.0, further increase of pressure ratio rapidly increased the base pressure for all configurations and free-stream Mach numbers studied until the base pressure was well above the jet-off values.

3. In general, increasing the angle of attack decreased the base pressure.

4. Total drag exhibited the same characteristics as boattail and base drag.

Lewis Flight Propulsion Laboratory
National Advisory Committee for Aeronautics
Cleveland, Ohio, February 17, 1954

REFERENCES

1. Katz, Ellis, and Stoney, William E., Jr.: Base Pressures Measured on Several Parabolic-Arc Bodies of Revolution in Free Flight at Mach Numbers from 0.8 to 1.4 and at Large Reynolds Numbers. NACA RM L51F29, 1951.

2. Cohen, Robert J.: Aerodynamic Characteristics of Four Bodies of Revolution Showing Some Effects of Afterbody Shape and Fineness Ratio at Free-Stream Mach Numbers from 1.50 to 1.99. NACA RM E51C06, 1951.

3. Chapman, Dean R.: An Analysis of Base Pressure at Supersonic Velocities and Comparison with Experiment. NACA TN 2137, 1950.

4. Faro, I. D. V.: Experimental Determination of Base Pressures at Supersonic Velocities. Bumblebee Rep. No. 106, Appl. Sci. Lab., Johns Hopkins Univ., Nov. 1949. (Contract Nord 7386, Bur. Ordnance, U.S. Navy.)

5. Hill, Freeman K. and Alpher, Ralph A.: Base Pressures at Supersonic Velocities. Jour. Aero. Sci., vol. 16, no. 3, Mar. 1949, pp. 153-160.

6. Charters, A. C., and Turetsky, R. A.: Determination of Base Pressure from Free-Flight Data. Rep. No. 653, Ballistic Res. Labs., Aberdeen Proving Ground, Mar. 30, 1948.

7. Love, Eugene S.: Aerodynamic Investigation of a Parabolic Body of Revolution at Mach Number of 1.92 and Some Effects of an Annular Jet Exhausting from the Base. NACA RM L9K09, 1950.

8. Cortright, Edgar M., Jr., and Schroeder, Albert H.: Preliminary Investigation of Effectiveness of Base Bleed in Reducing Drag of Blunt-Base Bodies in Supersonic Stream. NACA RM E51A26, 1951.

9. Schairer, George: Performance Characteristics of Jet Nozzles. Doc. No. D-12054, Boeing Airplane Co., Seattle (Wash.), July 25, 1951.

10. Cortright, Edgar M., Jr., and Schroeder, Albert H.: Investigation at Mach Number 1.91 of Side and Base Pressure Distributions over Conical Boattails Without and With Flow Issuing from Base. NACA RM E51F26, 1951.

11. Hearth, Donald P., and Gorton, Gerald C.: Investigation of Thrust and Drag Characteristics of a Plug-Type Exhaust Nozzle. NACA RM E53L16, 1954.

12. Van Dyke, Milton D.: First- and Second-Order Theory of Supersonic Flow Past Bodies of Revolution. Jour. Aero. Sci., vol. 18, no. 3, Mar. 1951, pp. 161-178.

13. Van Dyke, Milton D.: Practical Calculation of Second-Order Supersonic Flow Past Nonlifting Bodies of Revolution. NACA TN 2744, 1952.

14. Jones, Robert T., and Margolis, Kenneth: Flow over a Slender Body of Revolution at Supersonic Velocities. NACA TN 1081, 1946.

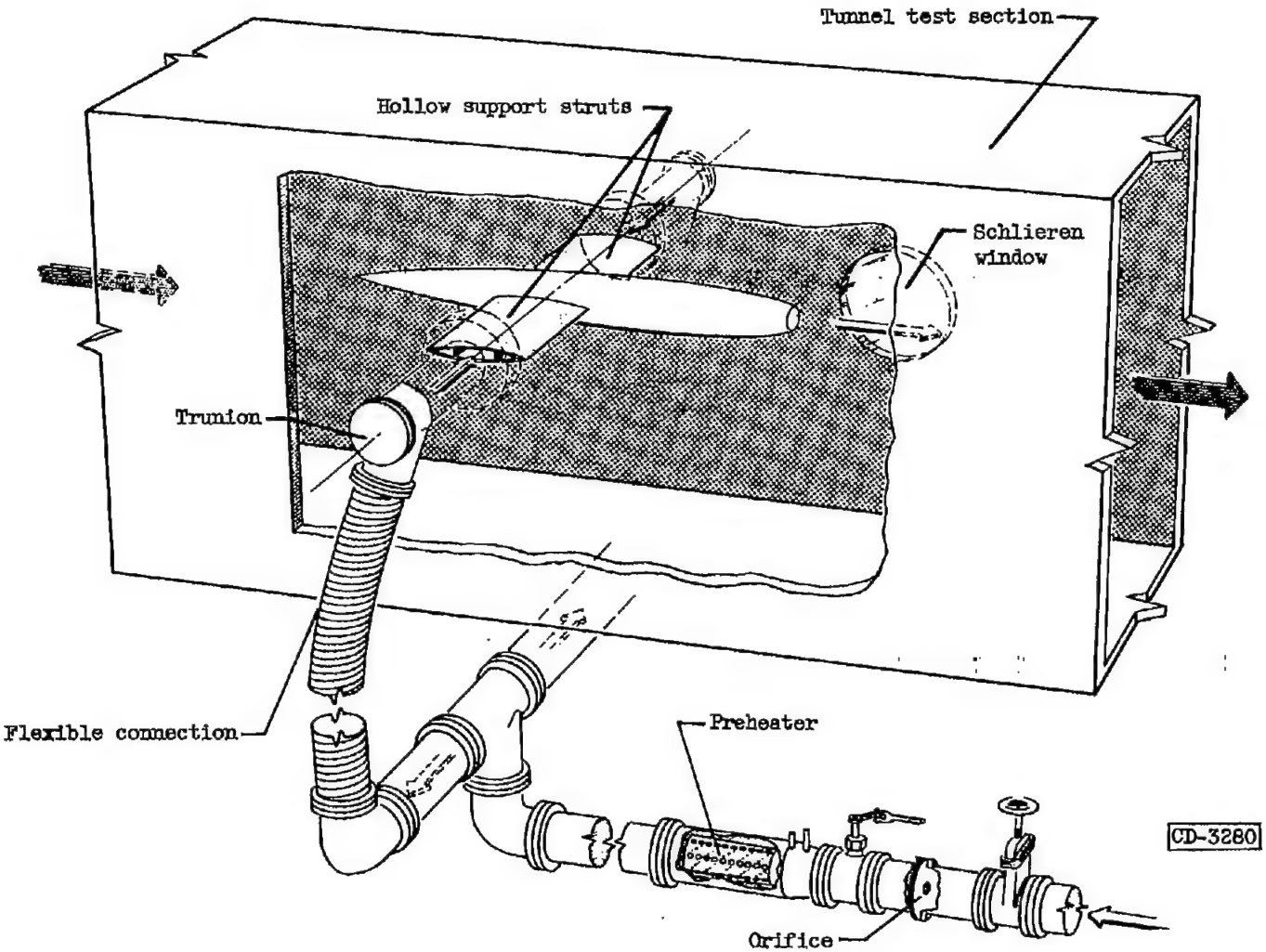

(a) Schematic drawing of jet-exit model in 8- by 6-foot test section.

Figure 1. - Experimental apparatus.

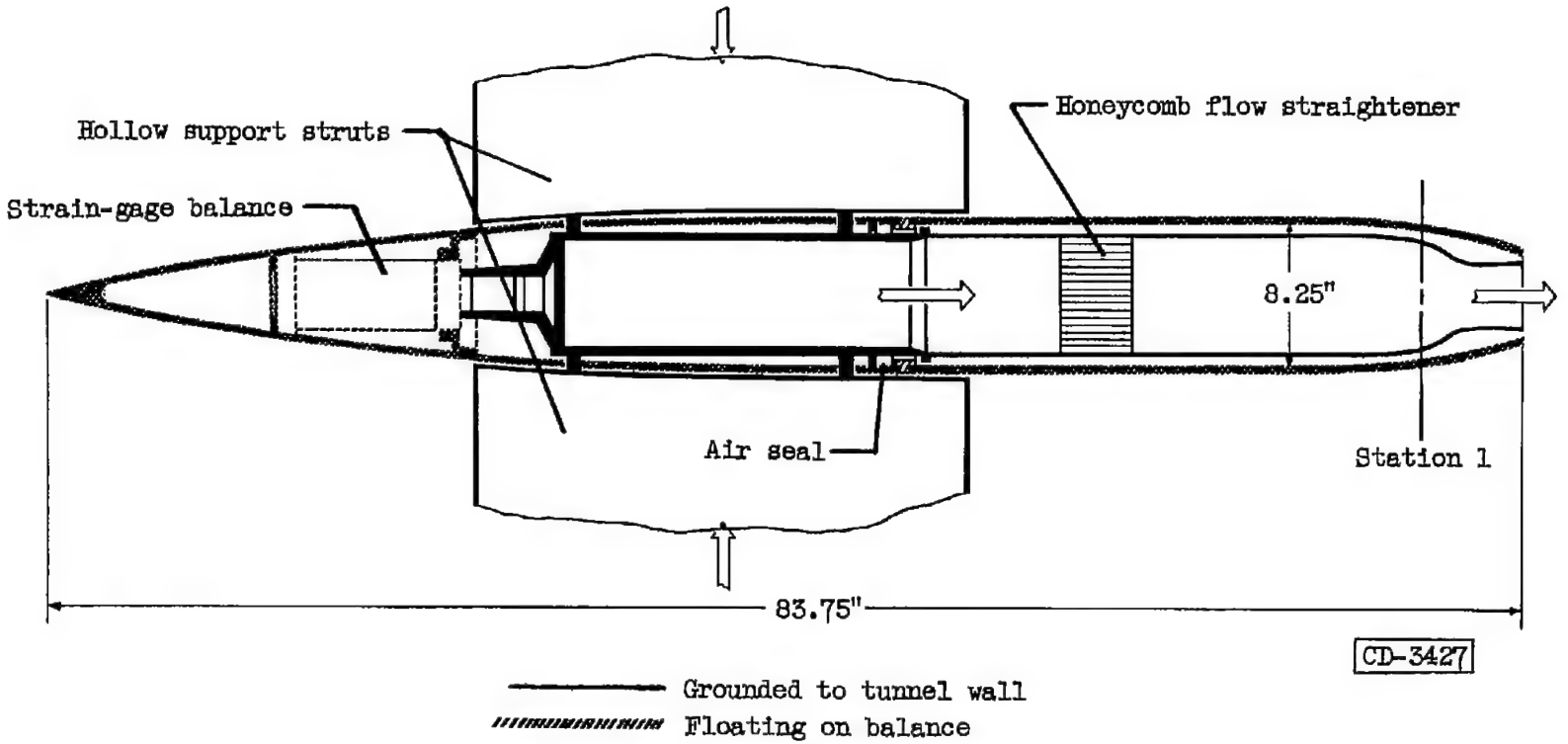

(b) Cross section of model.

Figure 1. - Continued. Experimental apparatus.

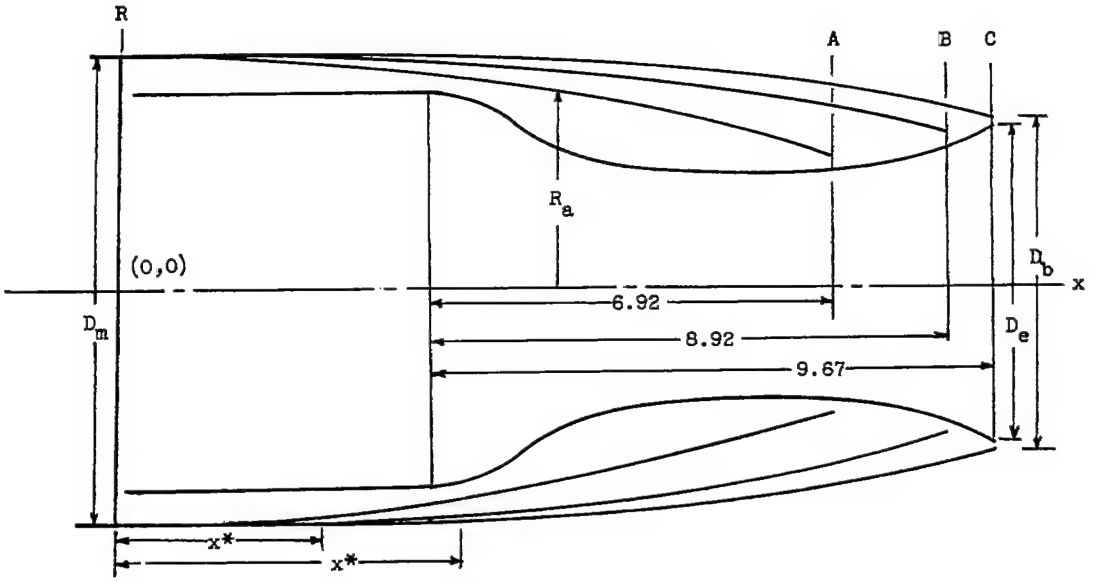

Equation of parabolic afterbody

$$R_a = 4.125 - \frac{4.125}{18^2}(x - x^*)^2$$

Nozzle coordinates	
x	R_N
0.00	3.500
2.00	3.500
4.00	3.500
[a]5.18	3.500
5.53	3.495
5.89	3.410
6.22	3.215
6.56	2.985
6.91	2.715
7.25	2.550
7.60	2.390
7.94	2.280
8.29	2.190
8.64	2.135
8.99	2.085
9.33	2.060
10.02	2.035
10.70	2.032
11.41	2.030
12.10	2.030
12.60	2.062
13.10	2.150
13.60	2.275
14.10	2.435
14.35	2.525
14.60	2.625
14.85	2.750

Nozzle	x* (b)	Design pressure ratio	Expansion ratio	Boattail length / Body length	Base diameter ratio, D_e/D_b	$\frac{D_e}{D_m}$
A	0	1.89	1.00	0.1445	0.902	0.492
B	3.40	5.75	1.44	.1278	.919	.590
C	5.25	9.10	1.83	.1146	.932	.667

[a]Start of nozzle contour.
[b]x* = length of cylindrical section to start of boattailing from reference axis (x = 0)

(c) Nozzle and boattail contours (dimensions in inches).

Figure 1. - Continued. Experimental apparatus.

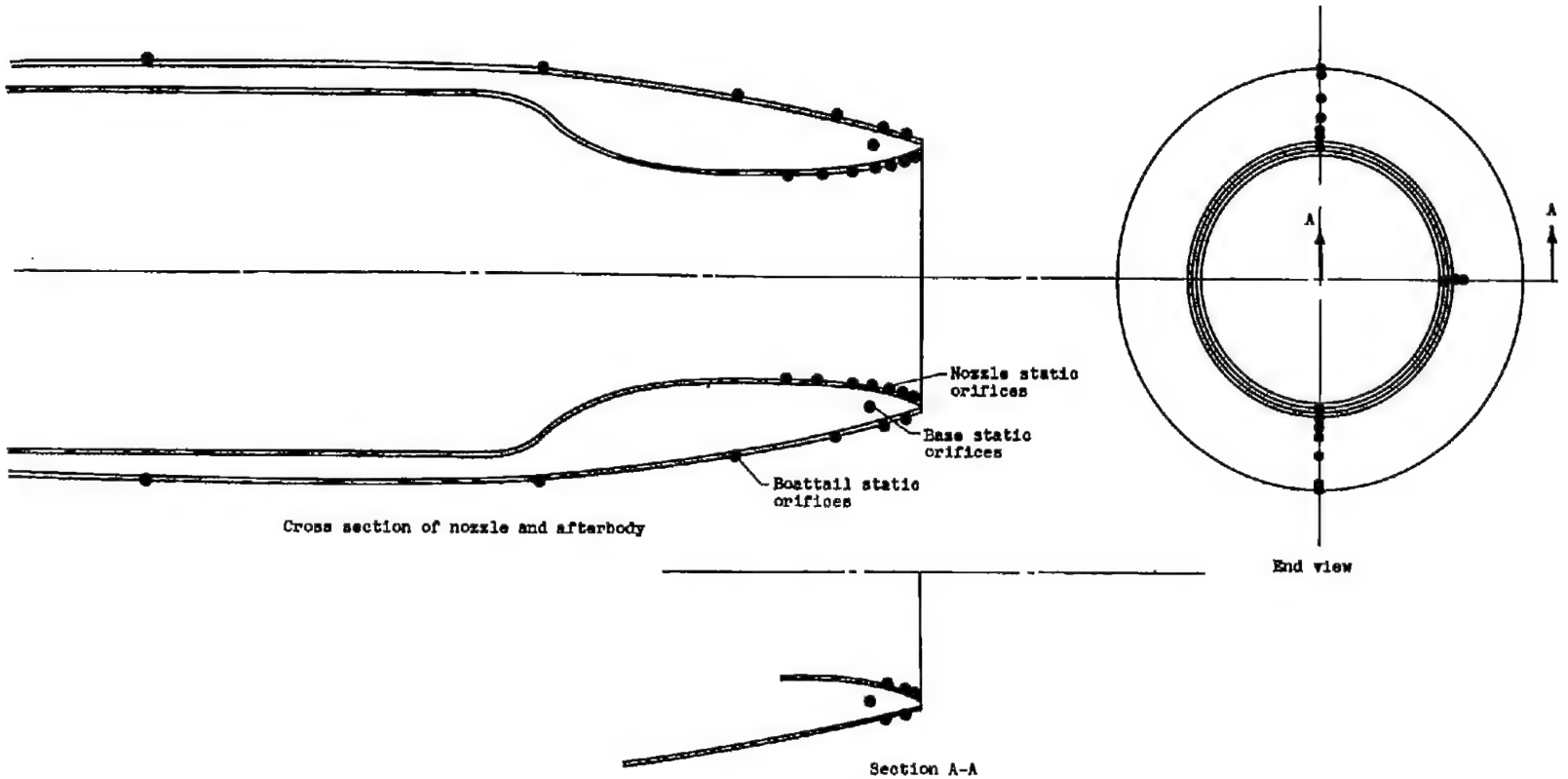

(d) Location of pressure-measuring orifices on nozzle and afterbody.

Figure 1. - Continued. Experimental apparatus.

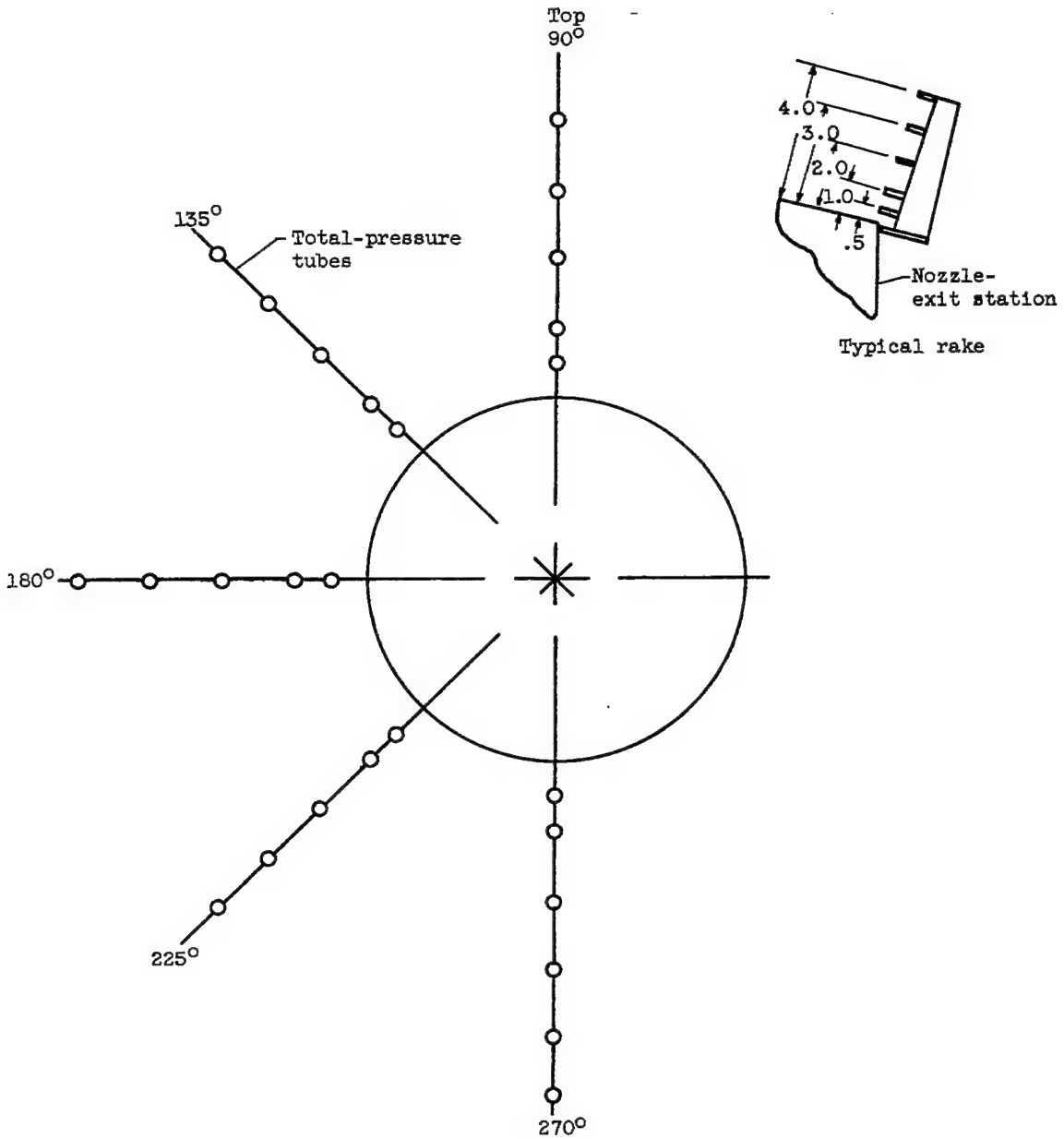

View of wake survey rakes from downstream station

(e) Position of boundary-layer rakes on afterbody (dimensions in inches).

Figure 1. - Concluded. Experimental apparatus.

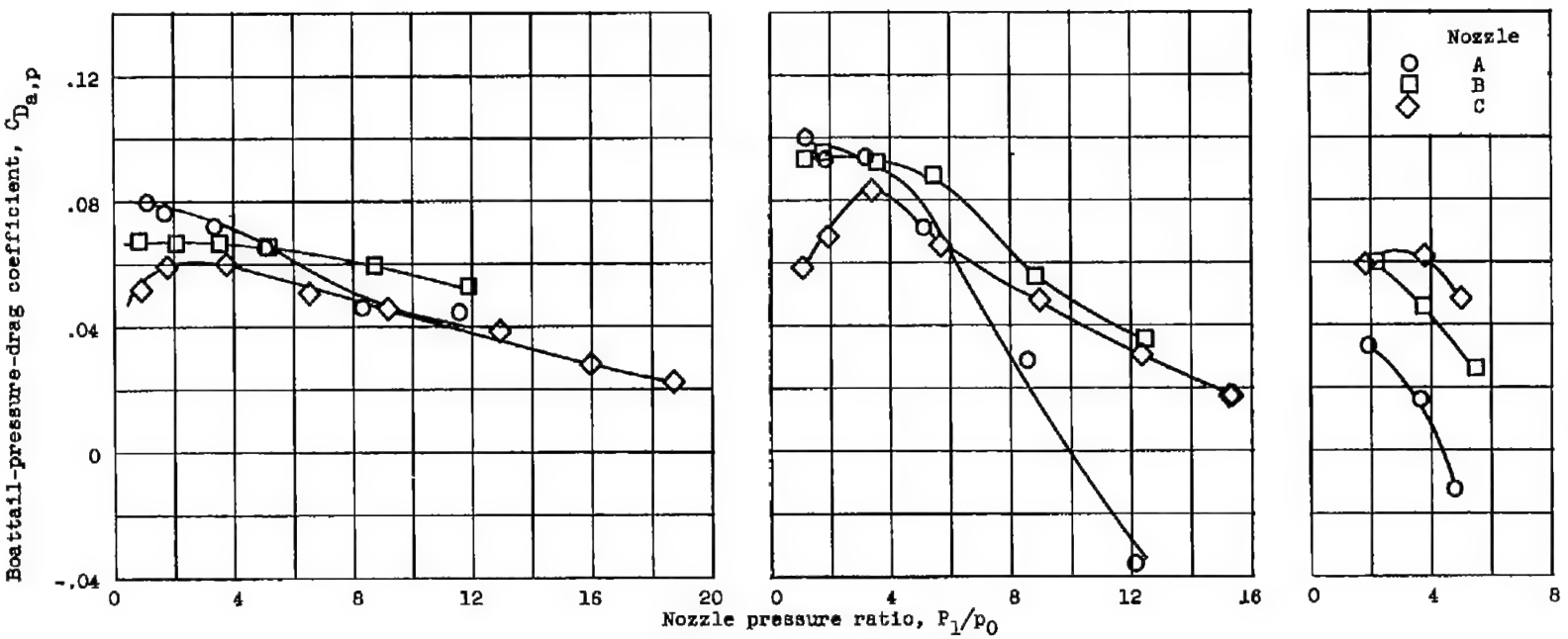

(a) Free-stream Mach number, 2.0.

(b) Free-stream Mach number, 1.6.

(c) Free-stream Mach number, 0.6.

Figure 2. - Effect of jet interference on boattail-pressure-drag coefficient at zero angle of attack.

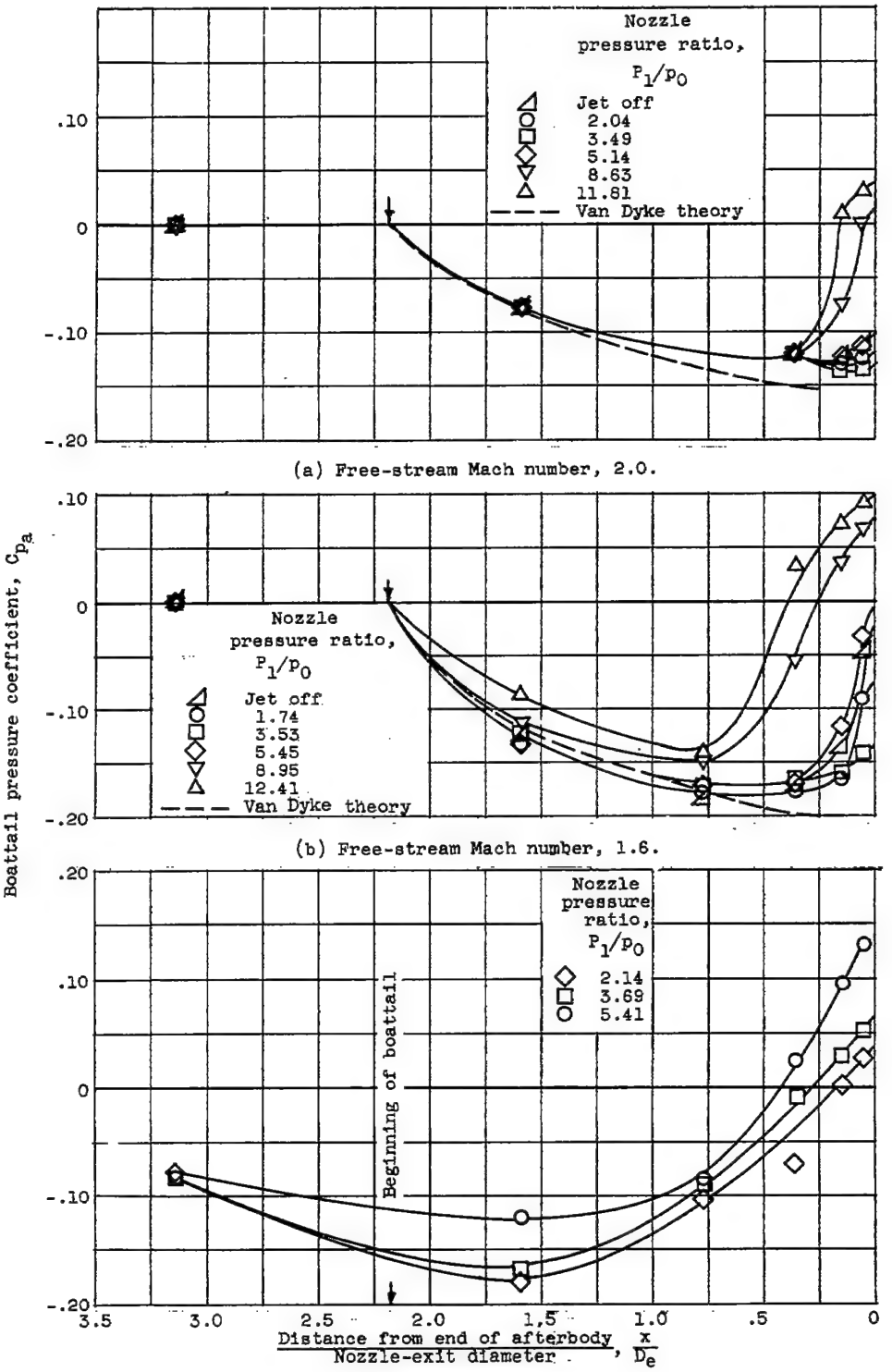

Figure 3. - Effect of jet interference on pressure distribution for convergent-divergent nozzle B.

(a) Free-stream Mach number, 2.0; nozzle pressure ratio, 1.15.

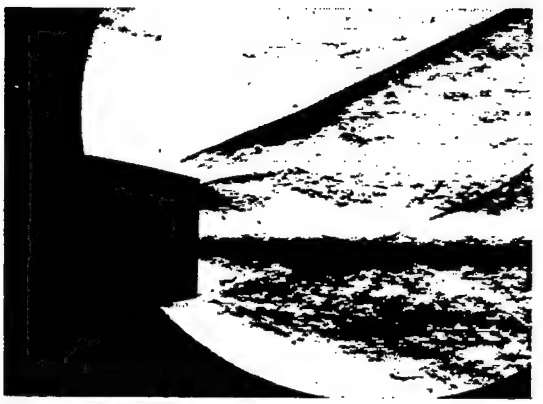

(b) Free-stream Mach number, 2.0; nozzle pressure ratio, 11.30.

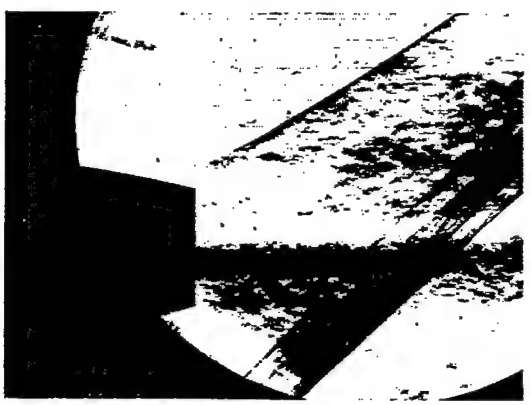

(c) Free-stream Mach number, 1.6; nozzle pressure ratio, 1.09.

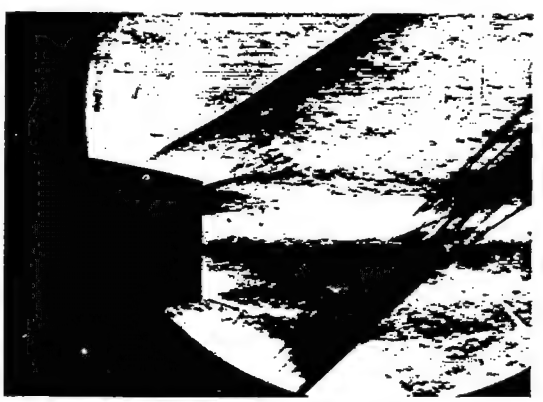

(d) Free-stream Mach number, 1.6; nozzle pressure ratio, 11.28.

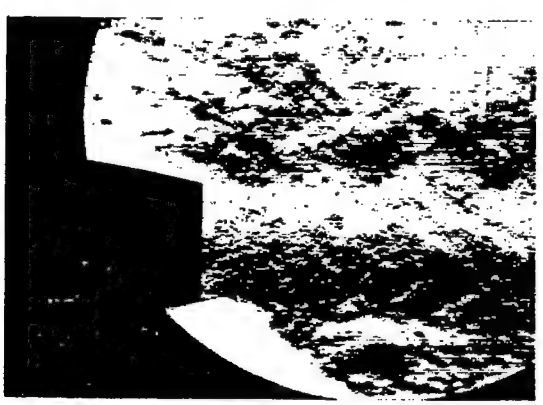

(e) Free-stream Mach number, 0.6; nozzle pressure ratio, 1.88.

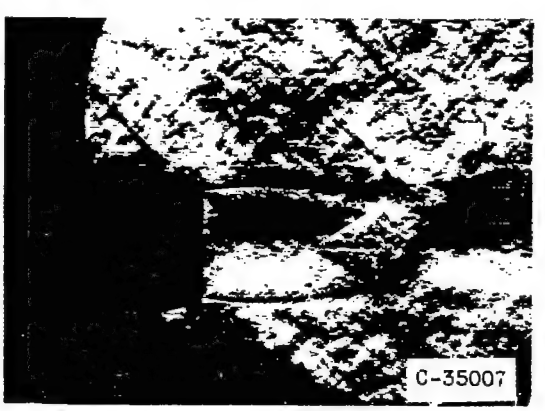

(f) Free-stream Mach number, 0.6; nozzle pressure ratio, 5.41.

Figure 4. - Schlieren photographs for nozzle B.

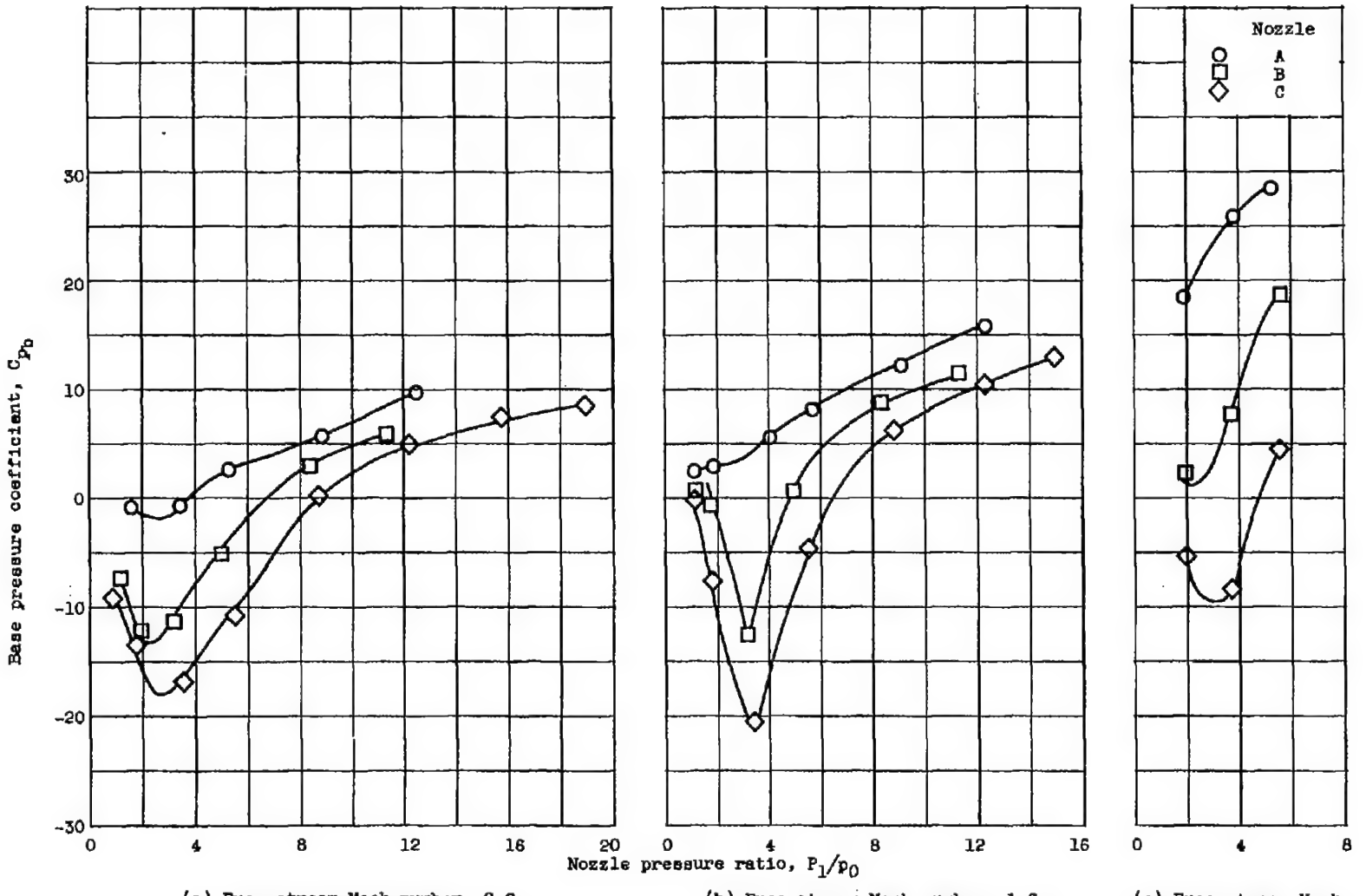

(a) Free-stream Mach number, 2.0.

(b) Free-stream Mach number, 1.6.

(c) Free-stream Mach number, 0.6.

Figure 5. - Effect of jet interference on base pressure coefficient.

(a) Free-stream Mach number, 2.0.

(b) Free-stream Mach number, 1.6.

Figure 6. - Effect of angle of attack on base pressure coefficient.

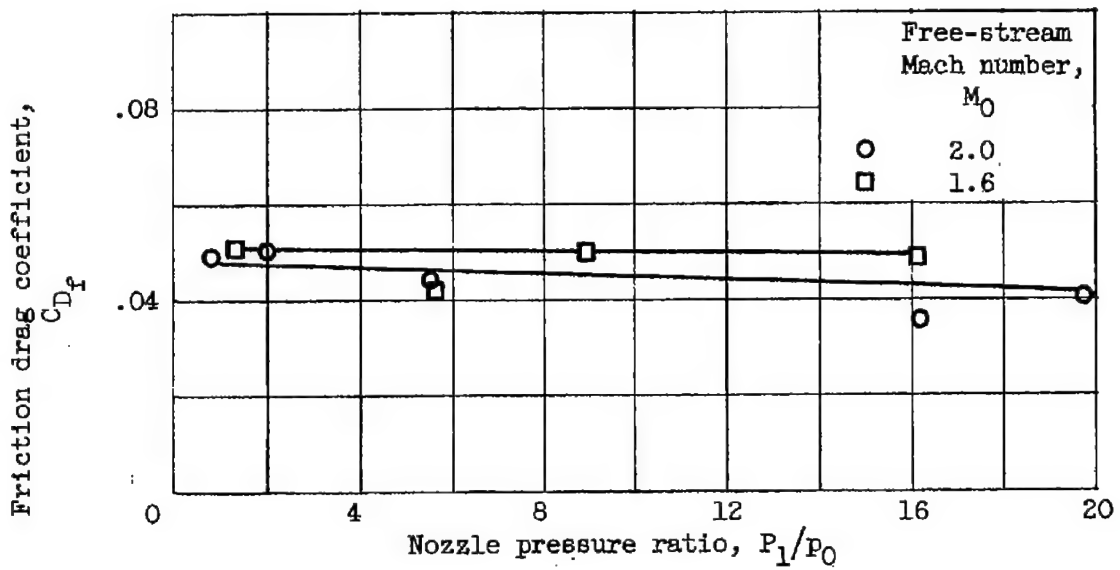

Figure 7. - Effect of jet interference on friction drag coefficient.

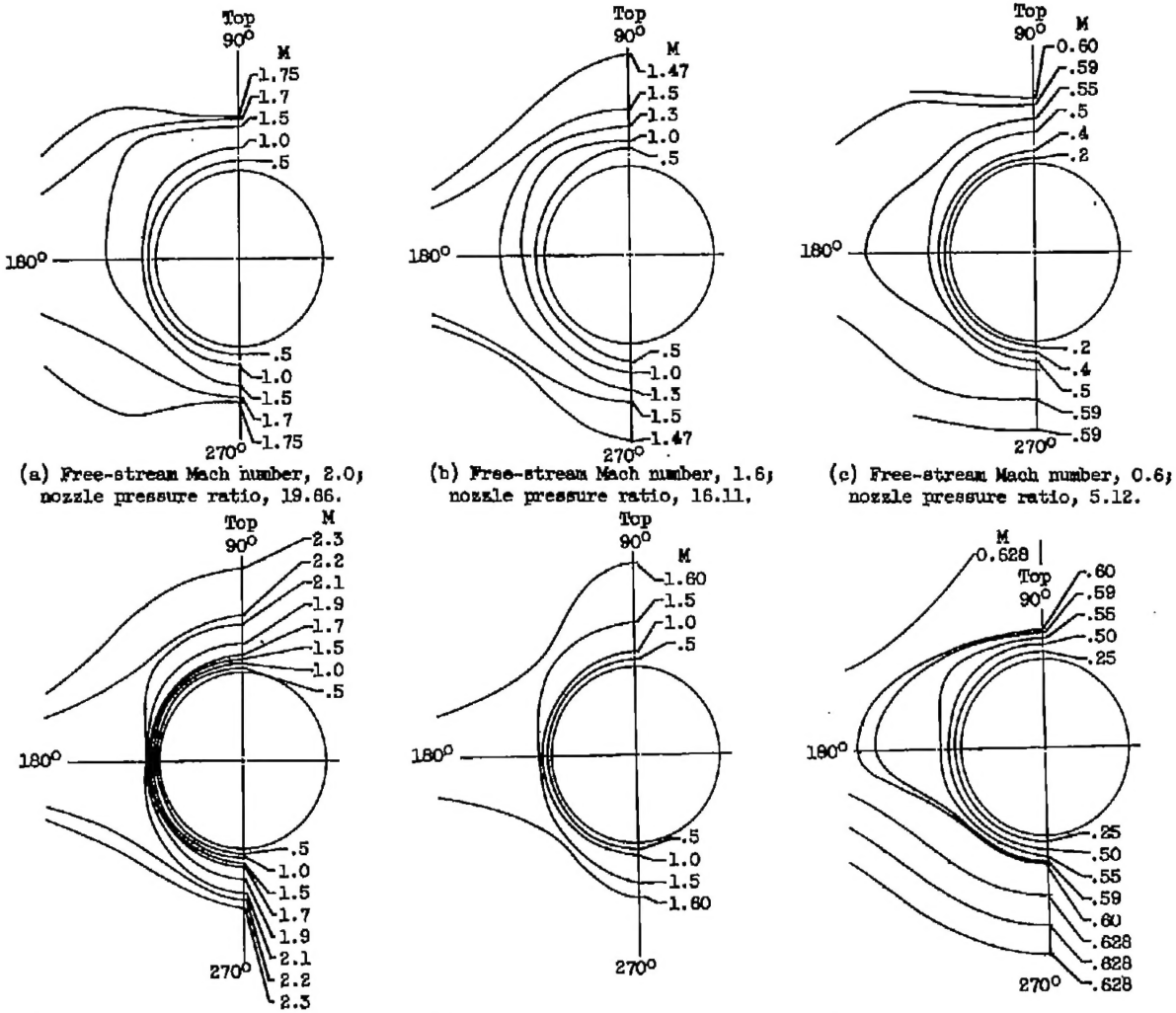

(a) Free-stream Mach number, 2.0; nozzle pressure ratio, 19.86.

(b) Free-stream Mach number, 1.6; nozzle pressure ratio, 16.11.

(c) Free-stream Mach number, 0.6; nozzle pressure ratio, 5.12.

(d) Free-stream Mach number, 2.0; nozzle pressure ratio, 0.83.

(e) Free-stream Mach number, 1.6; nozzle pressure ratio, 1.24.

(f) Free-stream Mach number, 0.6; nozzle pressure ratio, 1.94.

Figure 8. - Contour maps of Mach number M taken at wake survey station. Nozzle B; zero angle of attack.

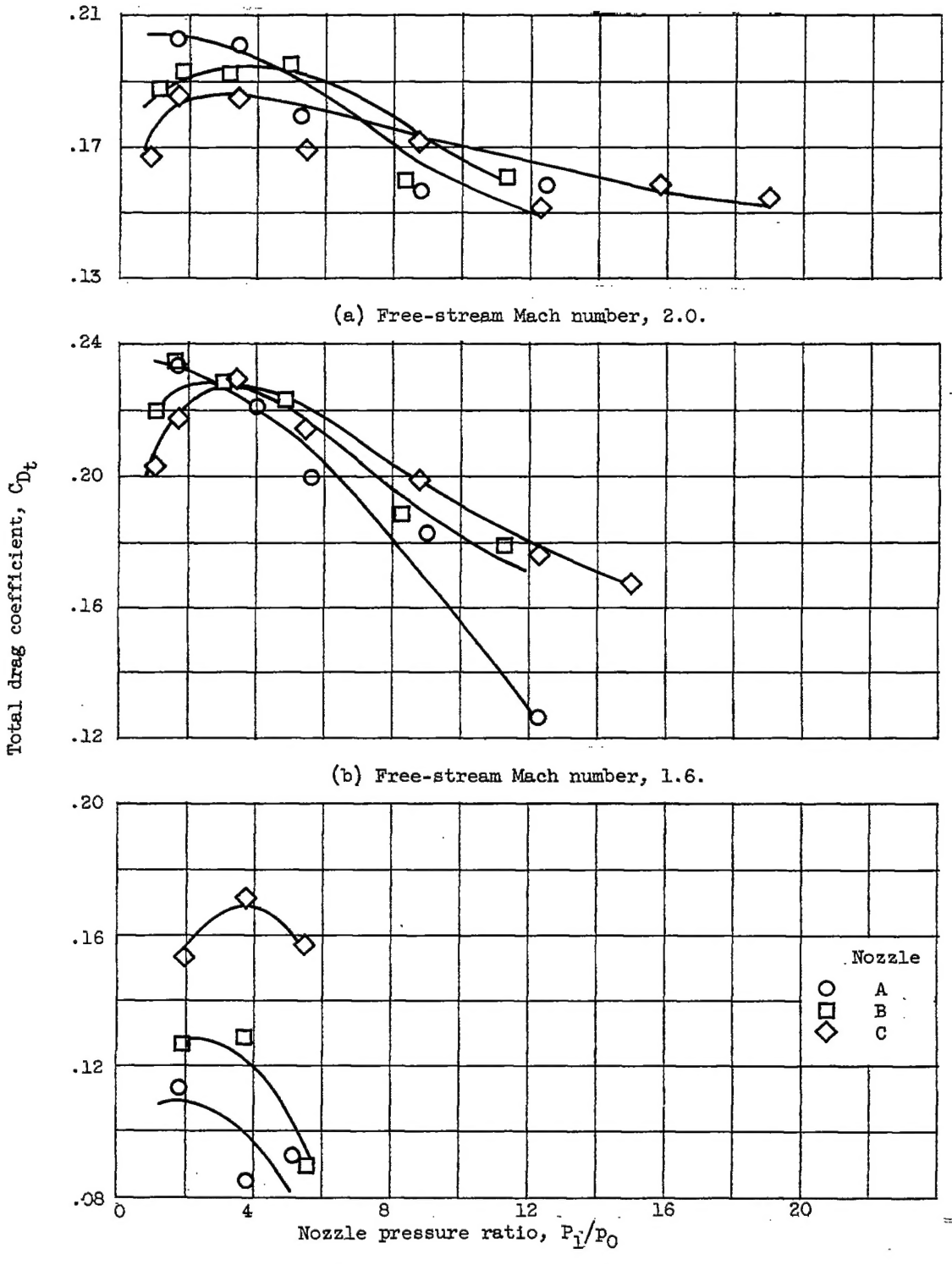

Figure 9. - Effect of jet interference on total drag.

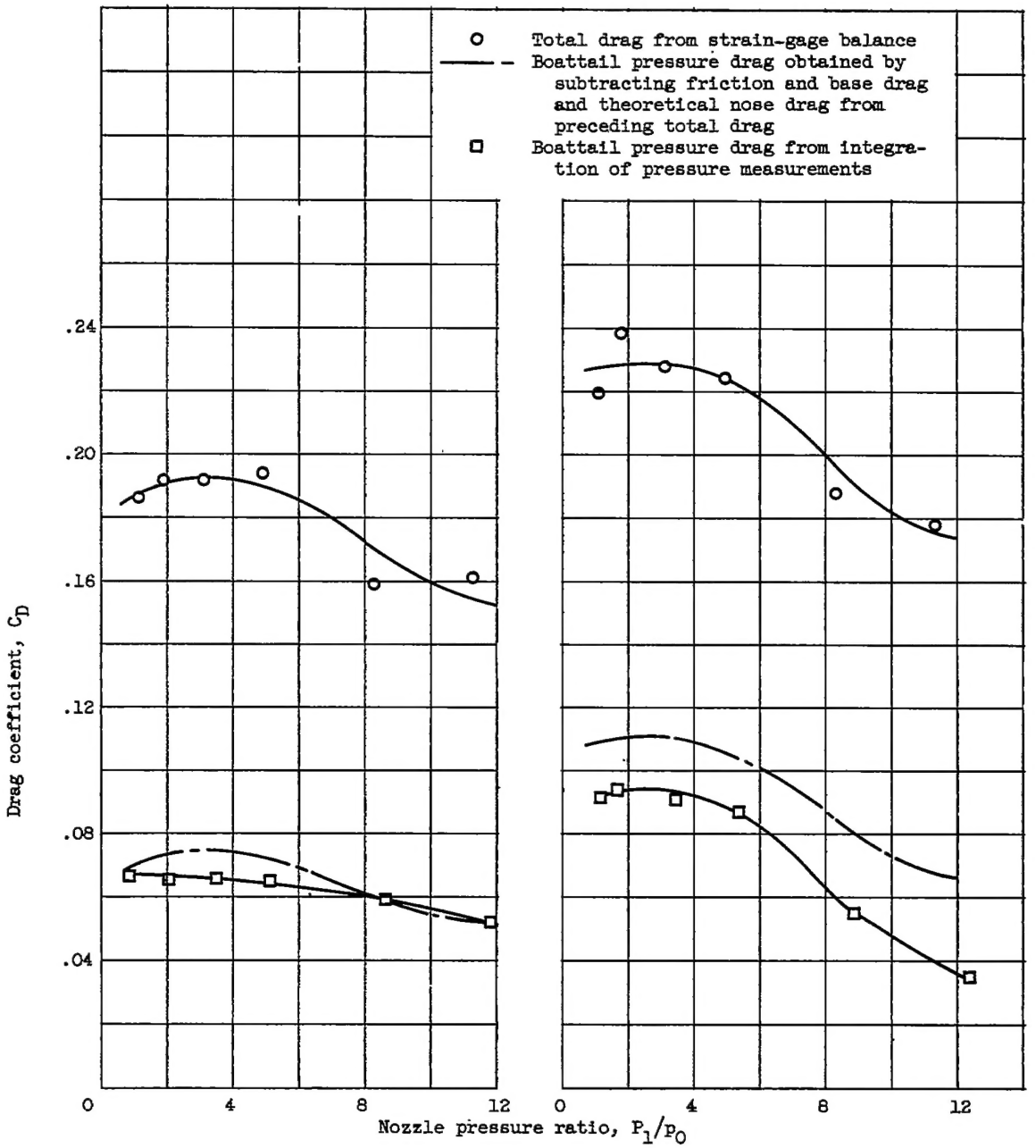

(a) Free-stream Mach number, 2.0. (b) Free-stream Mach number, 1.6.

Figure 10. - Comparison of boattail pressure drag obtained from two independent methods for convergent-divergent nozzle B.

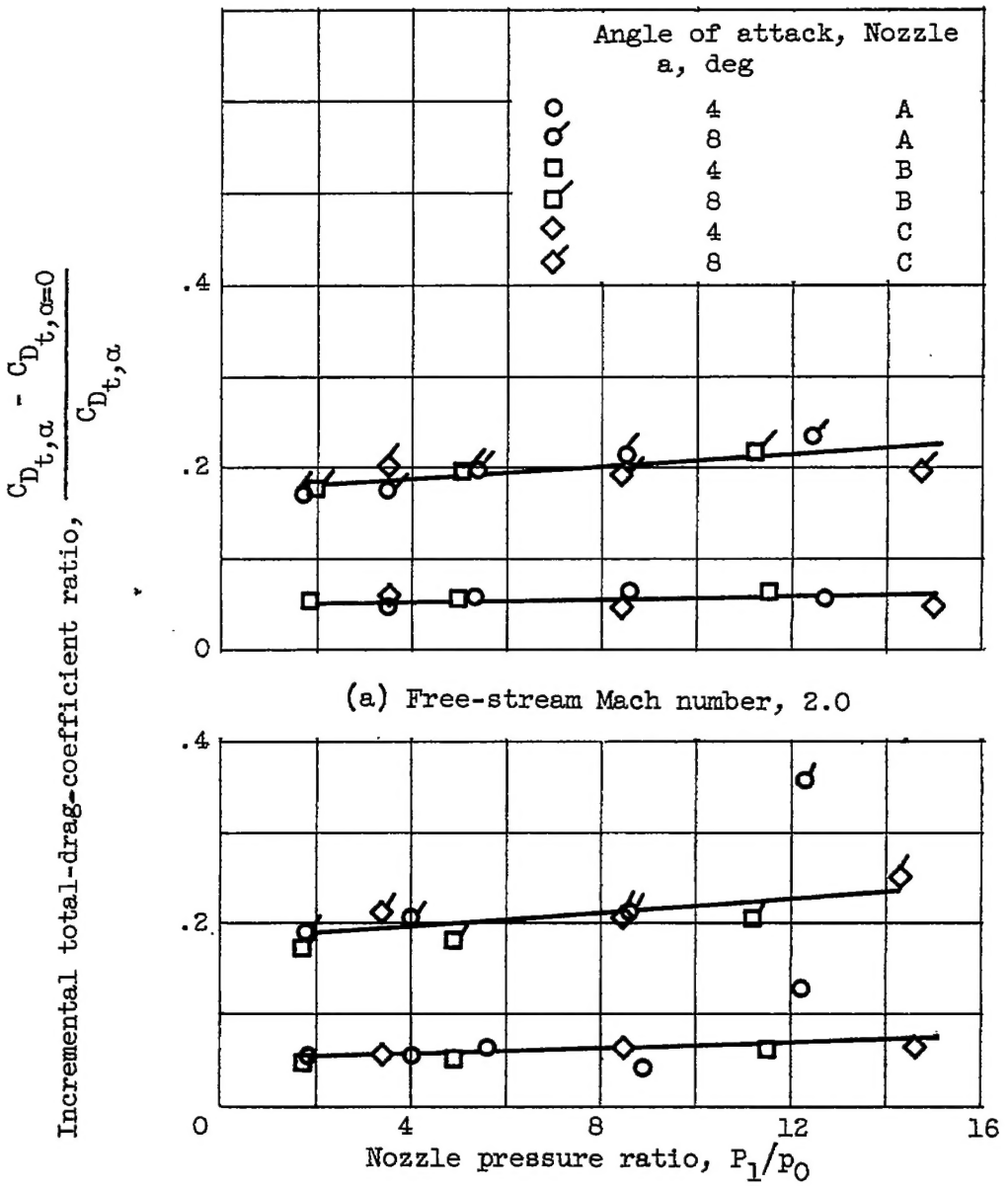

(a) Free-stream Mach number, 2.0

(b) Free-stream Mach number, 1.6.

Figure 11. - Effect of jet interference on total drag at angle of attack.

NACA-Langley - 4-19-54 - 325